DESIGN OF A NOVEL CONCEPT OF SYNCHRONOUS MOTOR FOR TORQUE RIPPLE IMPROVEMENT

Salim Asfirane, Sami Hlioui, H. Ben Ahmed, Lionel Vido, Mohamed Gabsi

DESIGN OF A NOVEL CONCEPT OF SYNCHRONOUS MOTOR FOR TORQUE RIPPLE IMPROVEMENT

Salim Asfirane[1], Sami Hlioui[1,2], Hamid Ben Ahmed[1,3], Lionel Vido[1,4], Mohamed Gabsi[1]

[1]SATIE Laboratory, ENS Cachan, 61 avenue du Président Wilson 94230 Cachan
salim.asfirane@satie.ens-cachan.com
[2]CNAM, 292 Rue Saint-Martin, 75003 Paris
sami.hlioui@satie.ens-cachan.com
[3]ENS Rennes, Campus de Ker lann, Avenue Robert Schuman, 35170 Bruz
[4]Cergy-Pontoise University, CNRS, 33 Boulevard du Port, 95000 Cergy-Pontoise
lionel.vido@u-cergy.fr

Abstract - In this paper, a novel design of synchronous machine is presented, the Multi-Stack Flux Modulating Machine (MSFModM). The MSFModM is made of 2 separate machines combined together into one multi-stack structure. The 2 combined stators share the same concentrated armature winding. A 2-D electromagnetic Finite Element Model (FEM) is built for a 3-phase 6/4 motor (6 stator teeth, 4 rotor teeth) and a Magnetic Equivalent Circuit (MEC) is used to evaluate the 3-D effect of the multi-stack machine and to correct the 2-D FEM flux linkage evaluation. The MSFModM concept is compared to a Biased Flux Permanent Magnet Motor (BFPMM). The two motors are supplied by three-phase sine wave currents and comparisons are carried out in terms of flux linkage, back-EMF and torque as the MSFModM exhibits a lower torque ripple.

Keywords – Double salient, permanent magnet, concentrated winding, torque ripple, multi-stack, magnetic equivalent circuit

1. INTRODUCTİON

For their cheap cost and robustness, Switched Reluctance Machines (SRM) have proved their value even in embedded applications [1], [2]. In order to keep the advantages of a passive rotor and to enhance performances, placing additional magnetic sources in the stator led to concepts like the doubly salient permanent magnet motor (DSPM) [3]–[6], the biased flux permanent magnet motor (BFPMM) [7], [8] or the Flux Switching Permanent Magnet Machine (FSPM). Most investigated FSPM in scientific literature are of a 12/8 or 12/10 configuration [11], [12] but for high speed applications, a low number of rotor poles is preferred. Electrical frequency becomes critical in high speed and is even higher with the increase of the number of rotor poles. Because of the saliency of the previously mentioned machine topologies, a low number of rotor poles often leads to high torque ripple. On this last aspect, torque ripple can be reduced using some geometry modifications. Hole punching technique was adopted on a 6/4 SRM in [9] and the multi-stack approach was used on a 6/4 (FSPM) in [10] in order to reduce harmonic content and cogging torque. Based on those criteria: robustness (passive rotor), a low number of rotor poles and torque ripple reduction, this paper deals with the innovative topology of the Multi-Stack Flux Modulating Machine (MSFModM). The MSFModM operating principle is described together with a methodology for the finite element model in 2-D of a 6/4 topology. Further, a Magnetic Equivalent Circuit (MEC) is used to evaluate 3-D effects induced by the multi-stack concept of the MSFModM structure on flux linkage. Finally, the MSFModM is compared to BFPMM for flux linkage, back-electromotive force (EMF), torque performance and torque ripple evaluation.

2. DESİGN CONCEPT AND OPERATİNG PRİNCİPLE

2.1. GEOMETRİC DESİGN

The MSFModM is a concept combining 2 separate BFPMM machines together into one multi- stack structure. A non-magnetic separation is used as flux barrier in between “half-stator a” and “half- stator b” of “half-machine a” and “half-machine b” respectively. The combined half-stators share the same concentrated armature winding and thus the phase windings are common to both half-machines. The back-EMF in each phase is resulting from the

sum of flux variations due to flux paths in each half-machine.

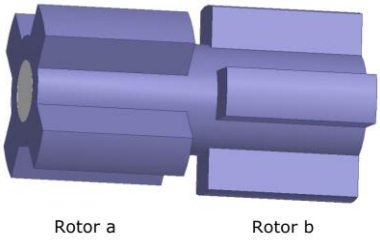

Fig. 1. Rotor of MSFModM (3-D view)

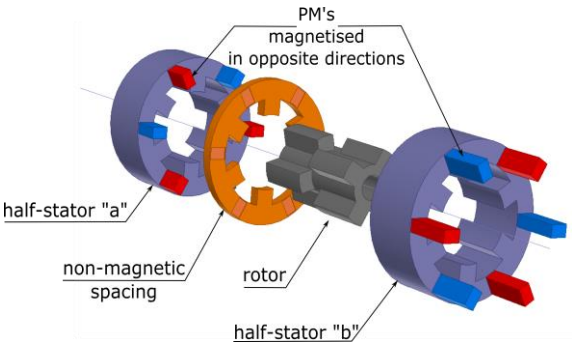

Fig. 2. MSFModM 3D exploded view

Furthermore, the toothed rotor is shifted from one half-machine to the other as it is illustrated on Fig. 1 for a 4-tooth rotor. Permanent Magnets (PM) are magnetized on the orthoradial direction and the magnetization direction is reversed from one half-machine to the other. Fig. 2 shows a 3-dimentional view of the MSFModM in the 3-phase 6/4 configuration.

2.2. MSFModM Operating Principle

By joining both half-machines into one multi-stack structure, we go from unidirectional flux variation to bidirectional thus going from homopolar configuration to heteropolar [13]. As the rotor of "half-machine b" is shifted by an angle of π/N_r, and the excitation is reversed from "half-machine a" to "half-machine b", the flux variation according to position in "half-machine b" is equivalent to the one in "half-machine a" with an offset angle of π/N_r and a -1 factor (due to the excitation being in the opposite direction). At an early design stage, the strong assumption that both half-machines are not magnetically coupled allows a two-dimensional study of the multi-stack structure (each half-machine on its own and superposition of results is operated afterwards). This assumption will be discussed later in more details. To illustrate this, a finite element model has been developed using Ansys-Maxwell [14] and flux linkage is evaluated in 2-D. First, when considering the position $\theta = 0°$ (see Fig. 3), "rotor a" is in the aligned position with regards to phase 1; while "rotor b" is in its unaligned position.

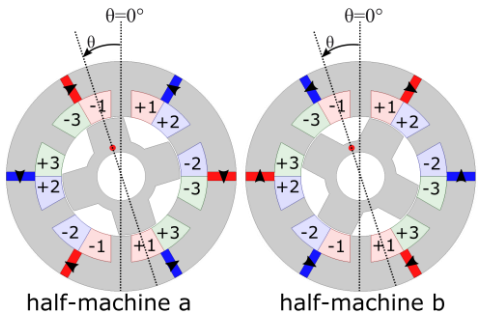

Fig. 3. Reference position

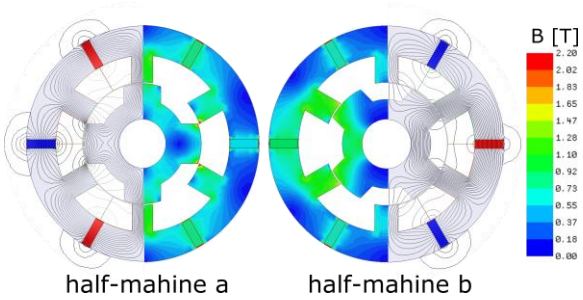

Fig. 4. Open-circuit induction distribution and flux lines at rotor position $\theta = 0°$

Fig. 4 shows, at rotor position $\theta=0°$, flux lines and magnetic induction distribution in the open-circuit situation. Fig. 5 shows, in the open-circuit situation, flux linkage for "half-machine a" and "half-machine b" as well as total flux linkage for the multi-stack machine.

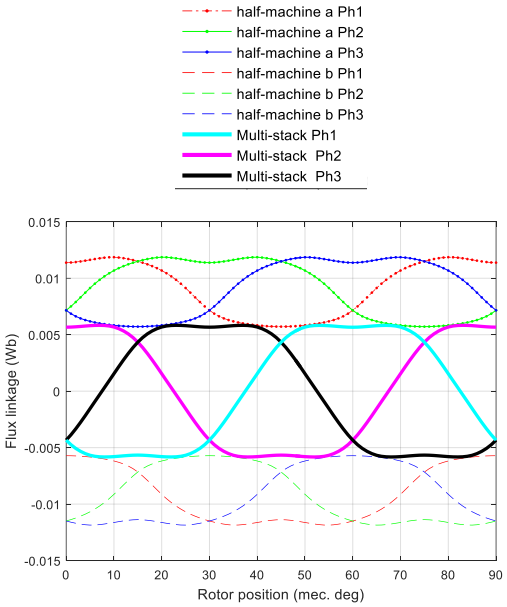

Fig. 5. Open-circuit flux linkage

When joining both half-machines, as they share the same armature coil, the total flux according to position in every phase is the sum of flux linkage of both half-machines at each position and then the

mean value of the total flux linkage over an electrical period is null. (See Fig. 5.) It is clear from Fig. 5 that there are 2 maximum flux positions and 2 minimum flux positions for this topology. In the open circuit situation, at rotor position θ = 10° (one maximum flux position) are illustrated on Fig. 6 flux lines and induction distribution. On Fig. 7, flux lines and induction distribution are given at rotor position θ = 35° (one minimum flux position).

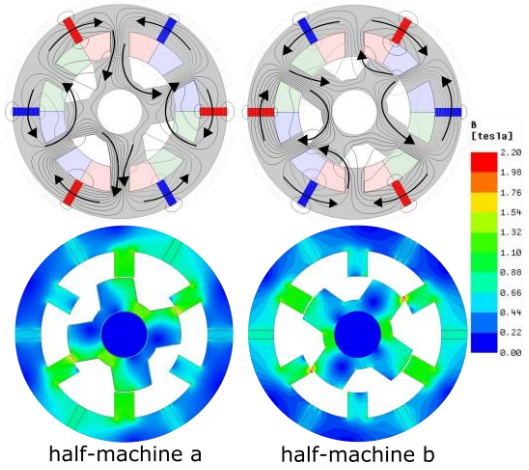

Fig. 6. Open-circuit flux lines and induction distribution at maximum flux position (θ = 10°)

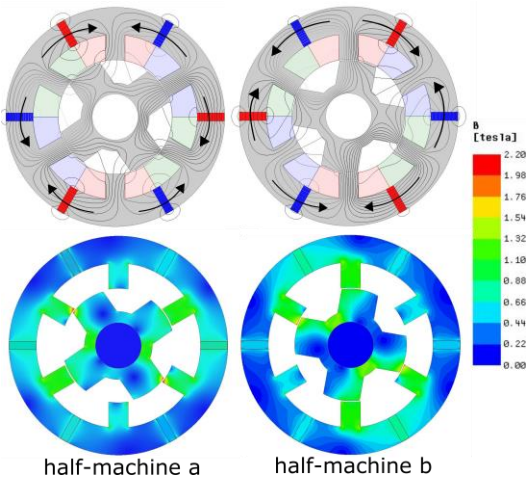

Fig. 7. Open-circuit flux lines and induction distribution at minimum flux position (θ = 35°)

3. PERFORMANCE COMPARİSON

3.1. MODEL AND PERFORMANCE CALCULATİON

The main geometric, magnetic and electric parameters of the BFPMM and the MSFMoM are given in table I. At first, flux linkage, back-EMF and torque are evaluated with a 2-D FEM model for the BFPMM. While for the MSFModM of the same parameters, it is easy to deduce these quantities as it was explained in the previous section.

I. MSFModM and BFPMM parameters

Parameter	**Value**
Turns per coil	72
Airgap	0.5 mm
Stator outer radius	45 mm
Split ratio	0.51
Stator pole arc	22.4°
Rotor pole arc	38.4°
PM thickness	11.2 mm
PM width	3.4 mm
Magnetic remanence	1.1 T
PM Relative permeability	1.04
Angular Speed	400 rpm
AC phase current	7.7 A

For the MSFModM, we still need to account for the flux "leakage" that is going to occur due to the axial 3-D flux path not concidered in a 2-D model. Furthermore, for the MSFModM to operate, it needs the non-magnetic spacing between the two half-stators. This spacing needs to be of a sufficient length so the flux path offered througth the aigap and rotor is less reluctant than the one throught the stator back-iron in the axial direction. Fig. 8 illustrates the axial flux path. The length of the non-magnetic spacing as well as correction factors for flux linkage are evaluated for each phase with the magnetic equivalent circuit (MEC) shown on Fig. 9.

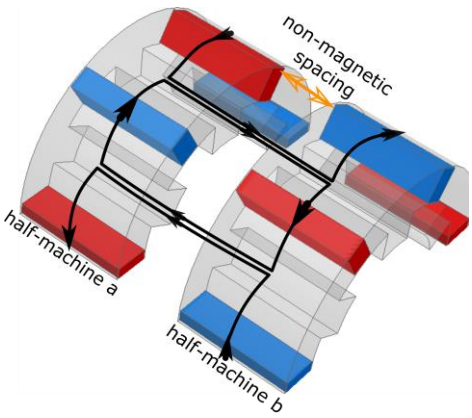

Fig. 8. Axial flux path

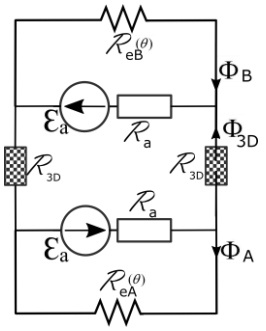

Fig. 9. MEC model for 3-D leakage flux correction

The elements of the magnetic equivalent circuit are listed in table II and are calculated as in (1) to (7).

II. MEC model parameters

Parameter	
R_{3D}	Reluctance of the 3-D flux path (non-magnetic spacing).
R_a	PM reluctance.
R_{eA}, R_{eB}	Reluctance of the airgap-rotor path, respectively "half-machine a" and "half-machine b".
Φ_A, Φ_B	Flux in "half-machine a" and "half-machine b" respectively.
Φ_{3D}	Flux in the 3-D flux path (non-magnetic spacing).

$$R_{3D} = \frac{l_{3D}}{\mu_0 S_{3D}} \quad (1)$$

$$R^j_{e\_i}(\theta) = \frac{R_{FE\_j}(\theta)}{\frac{1}{2}(L_{tot} - l_{3D})} \quad (2)$$

$$R_a = \frac{1}{\mu_{pm}} \frac{E_{pm}}{H_{pm}} \frac{1}{\frac{1}{2}(L_{tot} - l_{3D})} \quad (3)$$

$$\Phi^j_{FE\_i} = f(\theta, L_{tot}, l_{3D}) \quad (4)$$

$$R^j_{FE\_i}(\theta) = \frac{N^2}{L^j_{FE\_i}(\theta)} \quad (5)$$

$$S_{3D} = \frac{\pi}{6}\left(R^2_{ext\_s} - R^2_{cs}\right) \quad (6)$$

$$\varepsilon_a = \frac{E_{pm}}{\mu_{pm}} B_r \quad (7)$$

With:

ε_a : PM magnetomotive force
E_{pm} : PM width
H_{pm} : PM thickness
μ_{pm} : PM permeability
R_{ext_s} : Stator outer radius
R_{cs} : Stator yoke radius
l_{3D} : Non-magnetic spacing length
L_{tot} : Total length
N : Number of turns per coil
$\Phi^j_{FE\_i}$: Open circuit flux linkage given by FEM
$R^j_{FE\_i}$: Reluctance of the airgap-rotor path
$L^j_{FE\_i}$: Phase Inductance of the airgap-rotor path

i=1,2,3 and j = a, b for each phase in each half-machine respectively.

The airgap-rotor path reluctances are calculated via the FEM evaluation of phase inductance in the linear case as shown in (5). The 2-D reluctance (airgap-rotor path) for phase 1 in each half-machine are shown on Fig. 10.

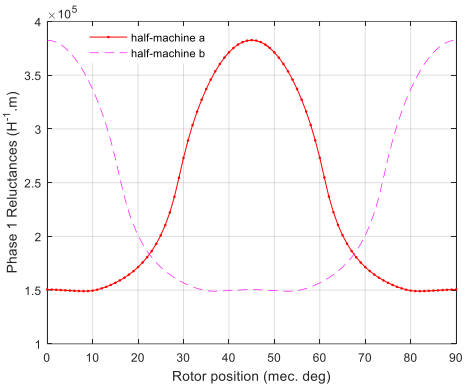

Fig. 10. Phase 1 Reluctance (FEM model)

To assemble 2 BFPMM's of reversed magnetisation, the phase flux linkage evaluated by the FEM model for each half-machine has to be corrected by the coefficients given in (8). These coefficients are determined by the MEC model as the ratio of flux going through the airgap-rotor path for a chosen value of the non-magnetic spacing length to the airgap-rotor path flux for an infinite l_{3D} value ie: when the 2 half-machines are not magnetically coupled. The correction takes into account both loss effects occurring in the MSFModM when compared to a BFPMM of the same total length. The loss of active length caused by non-magnetic spacing and the flux loss through non-magnetic spacing 3-D axial path.

$$k^j_i(\theta) = \frac{\Phi^j_i(\theta, R_{3D})}{\Phi^j_i(\theta, R_{3D} = \infty)} \quad (8)$$

k^j_i: Correction factor for 3-D flux loss and active length loss.

The flux linkage of each phase of the multi-stack machine is calculated as in (9) and finally the MSFModM torque is calculated according to (10).

$$\Phi_{MS\_i} = k^A_i(\theta)\Phi^A_{FE\_i} + k^B_i(\theta)\Phi^B_{FE\_i} \quad (9)$$

$$T_{MS} = \sum_{i=1}^{3} \frac{d\Phi_{MS\_i}}{d\theta} I_i \quad (10)$$

Where:

Φ_{MS_i}: Phase open circuit flux linkage of the MSFModM
T_{MS} : Torque of the MSFModM
I_i : Phase current

For the MSFModM of parameters given in table I, The optimal spacing length is calculated through multiple evaluations and on Fig. 11 are compared, for the same total lengths, average torque for the BFPMM and the MSFModM (at optimal non-magnetic spacing length).

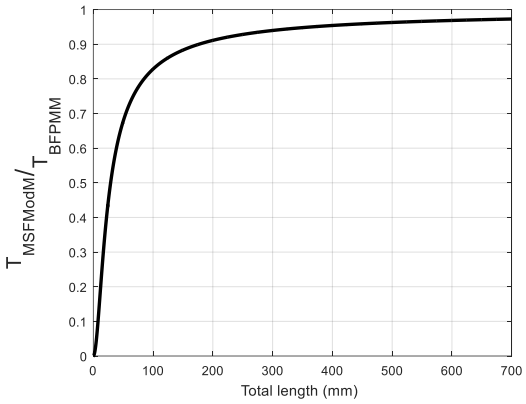

Fig. 11. Average Torque comparison

Only when total length reaches 180 mm that average torque of the MSFModM reaches 90 % of the BFPMM. This total length is then used for comparison. MSFModM additional parameters are given in table III and correction coefficients of phase 1 on both half-machines of the multi-stack are given on Fig. 12.

III. MSFModM additional parameters

Parameter	**Value**
Total length	180 mm
l_{3D}	8.6 mm

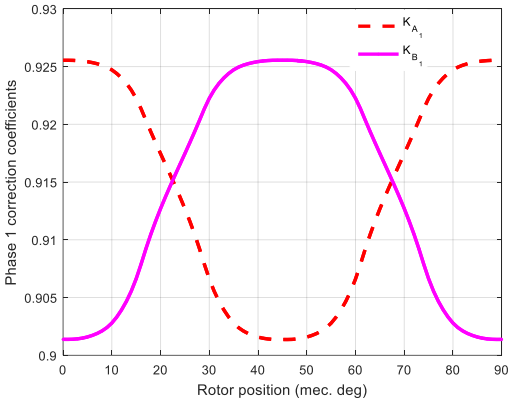

Fig. 12. Phase 1 correction coefficients for half-machine a and half-machine b

3.2. Results and Analysys

Fig. 13 shows open-circuit phase flux linkage for both BFPMM and MSFModM of the same parameters and active length. Fig. 14 and Fig. 15 show respectively open-circuit waveforms and spectrum. The MSFModM back-EMF is reduced in magnitude and harmonic order at 400 rpm.

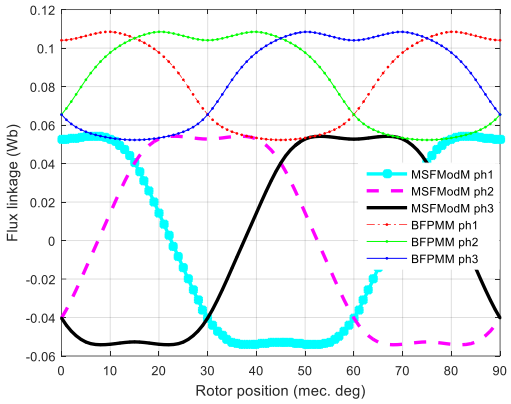

Fig. 13. Open-circuit flux linkage

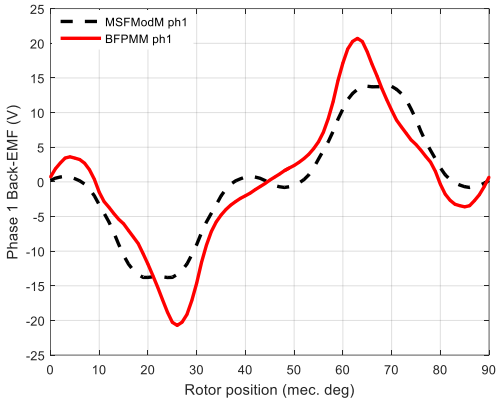

Fig. 14. Open-circuit phase back-EMF waveforms

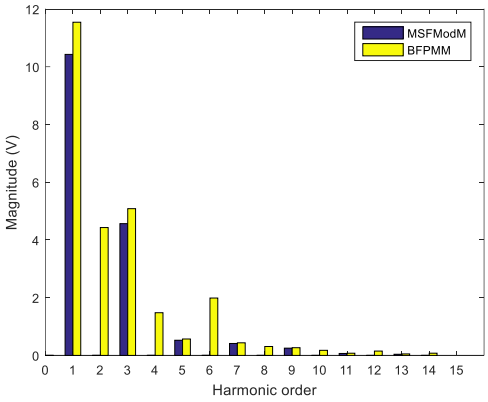

Fig. 15. Open-circuit phase back-EMF spectrum

When supplied with 3-phase sinewave current of magnitude given in table I in the previous section, MSFModM exhibits a lower average torque than the BFPMM of a same total length. This is due to the non-magnetic spacing (active length loss and flux leakage throught the 3-D path). Instant and average torque are given on Fig. 16.

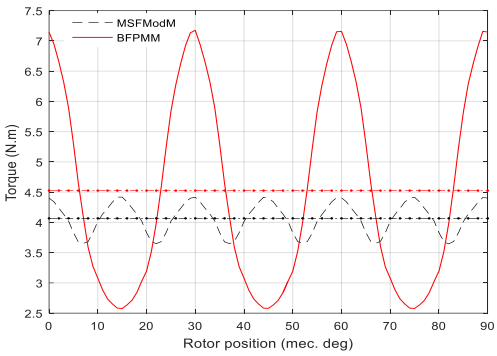

Fig. 16. Torque vs rotor position (I_{RMS}= 7.7 A)

The 10 % loss on average torque performance is a direct result of the loss af active conductors to the non-magnetic spacing length and flux leakage throught the axial path of the 3-D reluctance. However, the torque ripple is reduced. The MSFModM shows a noteworthy improvement as it goes from 101 % for the BFPMM to 19 % for the MSFModM despite the reduced average torque.

4. CONCLUSİON

Operating principles of a novel concept design of a passive rotor synchronous PM machine have been presented. A 2-D FEM model of the MSFModM is corrected using a MEC model to take into account the flux loss in the axial path (3-D effect) due to the non-magnetic spacing. Performances of the MSFModM have been compared to a simple BFPMM and torque ripple is greatly improved even if average torque is reduced. As perspectives for future studies, 3-D electromagnetic models will determine, with more precision, the interactions that could occur between the two half-machines and the influence of the non-magnetic spacing on developed torque.

REFERENCES

[1] M. Gabsi, A. D. E. Vries, M. L. E. Pincart, and Y. Bonnassieux, “Sine wave current feeding of doubly salient switched reluctance machines . Application to the car starter generator .,” in *ICEM’2004 Cracow, Poland , September*, 2004.

[2] K. M. Rahman and S. E. Schulz, “High performance fully digital switched reluctance motor controller for vehicle propulsion,” Industry Applications Conference, 36th IAS Annual Meeting. Conference Record IEEE, vol.1, pp. 18–25, 2001

[3] F. O. Hareb, B. Dunxin, and Z. Qionghua, “A New Type of Single Phase doubly Salient Permanent Magnet Motor,” 1955.

[4] Y. Li and C. Mi, “Doubly-salient permanent-magnet machine with skewed rotor and six-state commutating mode,” *Conf. Proc. - IPEMC 2006 CES/IEEE 5th Int. Power Electron. Motion Control Conf.*, vol. 2, no. 9, pp. 943–946, 2007.

[5] H. Hwang, S. Bae, and C. Lee, “Analysis and Design of a Hybrid Rare-Earth-Free Permanent Magnet Reluctance Machine by Frozen Permeability Method,” *IEEE Trans. Magn.*, vol. 52, no. 7, pp. 1–4, 2016.

[6] Thomas A Lipo; Yue Li, “A Doubly Salient Permanent Magnet Motor Capable of Field Weakening,” *Proc. - Power Electronics Specialists Conf., PESC '95*, IEEE 1995.

[7] J. T. Shi, Z. Q. Zhu, D. Wu, and X. Liu, “Influence of flux focusing on electromagnetic torque of novel biased flux PM machines,” *Proc. - 2014 Int. Conf. Electr. Mach. ICEM 2014*, pp. 523–529, 2014.

[8] D. Wu, J. T. Shi, Z. Q. Zhu, and X. Liu, “Electromagnetic performance of novel synchronous machines with permanent magnets in stator yoke,” *IEEE Trans. Magn.*, vol. 50, no.9, 2014.

[9] J. X. Shen and W. Z. Fei, “Permanent magnet flux switching machines - Topologies, analysis and optimization,” *Int. Conf. Power Eng. Energy Electr. Drives*, vol. 5, pp. 352–366, 2013.

[10] W. Hua, Z. Q. Zhu, M. Cheng, Y. Pang, and D. Howe, “Comparison of flux-switching and doubly-salient permanent magnet brushless machines,” *2005 Int. Conf. Electr. Mach. Syst.*, vol. 1, p. 165–170 Vol. 1, 2005.

[11] G. Li, J. Ojeda, S. Hlioui, E. Hoang, M. Lecrivain, and M. Gabsi, “Modification in rotor pole geometry of mutually coupled switched reluctance machine for torque ripple mitigating,” *IEEE Trans. Magn.*, vol. 48, no. 6, pp. 2025–2034, 2012.

[12] D. Bobba, Y. Li, and B. Sarlioglu, “Design Optimization for Reducing Harmonic Distortion of Flux Linkage in Low Pole Flux-Switching Permanent Magnet Machines,” in *IEEE Transportation Electrification Conference and Expo (ITEC)*, 2016, pp. 1–6.

[13] L. Vido, Y. Amara, M. Gabsi, M. Lécrivain, and F. Chabot, “Compared performances of homopolar and bipolar hybrid excitation synchronous machines,” *Conf. Rec. - IAS Annu. Meet. (IEEE Ind. Appl. Soc.*, vol. 3, pp. 1555–1560, 2005.

[14] ANSYS®, “Electromagnetics Suite, Release 16.2.” .